Iranian Journal of Catalysis 9(2), 2019, 121-132

IRANIAN JOURNAL OF CATALYSIS

Optimization and modeling of photocatalytic degradation of Direct Blue 71 from contaminated water by TiO_2 nanoparticles: Response surface methodology approach (RSM)

Mohamadreza Massoudinejad[a], Mohsen Sadani[a], Zeinab Gholami[b], Zeinab Rahmati[c], Masoume Javaheri[c], Hassan Keramati[d], Mansour Sarafraz[e], Moayed Avazpour[c,*], Sabah Shiri[f,*]

[a]*School of Public Health and Safety, Shahid Beheshti University of Medical Sciences, Tehran, Iran.*
[b]*Student Research Committee, School of Public Health, Tehran University of Medical Sciences, Tehran, Iran.*
[c]*Department of Environmental Health Engineering, School of Public Health, Ilam University of Medical Science, Ilam, Iran.*
[d]*Department of Environmental Health Engineering, School of Public Health, Semnan University of Medical Sciences, Semnan, Iran.*
[e]*Student Research Committee, School of Public Health and Safety, Shahid Beheshti University of Medical Sciences, Tehran, Iran.*
[f]*Department of Chemistry. Payame Noor University. P.O. Box 19395-4697, Tehran, Iran.*

Received 22 May 2018; received in revised form 21 August 2018; accepted 2 September 2018

ABSTRACT

In the current survey, the removal of dye from contaminated water was studied by photocatalytic degradation using TiO_2 nanoparticles with respect to pH, TiO_2 dosage, reaction time, temperature and initial dye concentration. TiO_2 nanoparticles were investigated by XRD, FESEM and FT-IR. The RSM was chosen to study the composition effects of input independent factors and one dependent output response (removal efficiency). The P-value (2.2×10^{-16}), F-value (1832), R^2 (multiple R-squared: 0.9985, adjusted R-squared: 0.9972), and lack of fit (0.432) indicate that the reduced full second order model is highly significant for dye removal by TiO_2 nanoparticles. The maximum percentage removal of dye, 90.2%, was achieved at optimum operating conditions including pH=6.5, TiO_2 dose (1.2 g L^{-1}), contact time (67.5 min), temperature (40 °C), and dye concentrations (55 mg L^{-1})), respectively. The maximum removal efficiency was calculated to be 100%, using regression coefficients derived from the model and the Solver "Add-ins". The results indicated that the TiO_2 photocatalyst was very proper for the removal dye from contaminated water, and it had good efficiency in eliminating textile dyes.

Keywords: *TiO_2, Photocatalyst, Degradation, Direct blue 71, Optimization, RSM.*

1. Introduction

Today water pollution as a result of industrialization and fast population growth is transformed into an environmental health risk to mankind [1]. Annually about 7×10^5 tons of dyes are manufactured in worldwide and dyes pollutants produced by various industries such as textile, leather, paper, ceramic, cosmetics, ink and plastic are entered into the environment [2-4].

*Corresponding authors.
Email addresses:
m_f_1859@yahoo.com (M. Avazpour)
sabahshiri5@yahoo.com (S. Shiri)

Dyes and products of their degradation are often toxic, non-biodegradable, non-consistent and in some cases even mutagenic and carcinogenic to humans and animals [5, 6]. Releasing colored wastewater into the free water causes eutrophication and interference in the ecology of water bodies, affecting on the intensity of photosynthesis of aquatic plants and finally creating damage to the environment [7-9]. Treatment of wastewater containing dyes is often more important than the other substances, because the dyes are recalcitrant organic molecules that are resistant to aerobic digestion, stable to light, heat and oxidizing agents [10-13]. Because of the dye resistance against biodegradation, often for the removal of dyes, physical and chemical

methods have been used such as adsorption, coagulation, flocculation, photolysis, chemical oxidation, ozonation, membrane filtration etc. [14]. Physical methods only transfer the contaminant to another phase, so they are non-destructive and produce a potentially hazardous effluent [15,16]. Since chemical methods require the high dosage of chemicals, they are expensive and produce a large quantity of sludge [17-19]. Advanced oxidation processes (AOPs) are based on the generation of very reactive and oxidizing free radicals, especially hydroxyl radicals [20-22]. In general, AOPs typically include all processes, in which Hydroxyl radical ($OH^{\cdot}$) is created as an oxidizer for the decomposition of pollutants [23-27]. The process of TiO_2/UV is one of the newest and most efficient methods for the treatment dye pollutants. In this photocatalytic process, the nanoparticles of TiO2 due to the high oxidation power, photochemical stability, large surface area to volume ratio, low toxicity and low cost, are widely used as catalysts in photocatalysts reactions [28-32]. The statistical response surface methodology (RSM) was used for investigation of effects of various parameters, determination of the interactions of the experimental variables and reduction of the number of required experiments [33]. This software is a mathematical and statistical technique that was used in the statistical design of the experiments, and optimize the operating conditions in independent variables [34]. In general, the purpose of this work is the study of characterization of TiO_2 nanoparticles used for removal direct blue 71 dye from contaminated waters by the photocatalytic oxidation process. Moreover, RSM was used for predicting and modeling the complicated relations between input-independent factors and determining the dye removal efficiency (Y) under the optimum operational conditions.

2. Experimental

2.1. Materials

To provide all of the chemicals and standard solutions, De-ionized water was used. Nanoparticles of P-25 TiO_2 (mainly in anatase form), with an average particle size less than 30 nm, the specific surface area (BET) of 50±15 m^2/g and purity greater than 99.5% from Degussa (Germany) were applied as the photocatalysts. The direct blue-71 dye from Alvan Sabet in Iran, with the chemical structure $C_{40}H_{28}N_7NaO_{13}S_4$ and a molecular weight of 965.94 g/mol was used as the sorbate in this study. To immobilize TiO2 on Borosilicate glass plates (150mm × 150mm), commercially available Titania powder such as aeroxide P25 is used and mixed with a solvent. Coating was done by pipetting methods. In pipetting, the substrate was then left to dry until most of the solvent evaporated. After sintering at high temperature (400-600 °C), the film will adhere to the substrate [35]. The distance between the UV lamps and TiO_2 films is 1.5 cm.

2.2. Photocatalytic experiments

The reactor used for the photocatalytic oxidation of DB-71 dye by UV/TiO_2 process is shown in Fig. 1. This reactor consists of two outer and inner parts, A UV-lamp with 128 W medium-pressure, 220 V and the maximum wavelength at 247.3 nm as the radiation source is located in the inner part. The outer portion of the reactor should contain 2 L solution for keeping the solution at 25±2 °C. All irradiation experiments of dye solution were done by stirring 1000 ml of dye solution with immobilized TiO_2. During the experiment, the solution in the reactor was constantly stirred. After providing the Stock solution (1000 mg/L) of DB-71, photodegradation dye experiments were done in a batch reactor by assessing the effects of pH (2 to 11), initial dye concentrations (10 to 100 mg L^{-1}), contact time (15 to 120 minutes), TiO2 dose (0.2 to 1.2 g L^{-1}) and temperature (20 to 60 °C). According to five variables of the pH, TiO_2 dose, contact time, temperature dye and concentration, to accomplish the tests, 62 runs were specified using the software R. dye concentrations of the samples were determined by spectrophotometer (DR5000, HACH LANGE, USA) according to the standard method at a wavelength of 594 nm [36]. For each experiment, the dye removal percentage (R %) was calculated using Eq. (1) :

$$R = \frac{C_0 - C_t}{C_0} \times 100 \quad (1)$$

Where C_0 is the initial dye concentration and C_t, is the concentration of dye at intervals of the irradiation time. The surface morphology and characteristics of P-25 TiO_2 nanoparticles were investigated using XRD, FESEM and FT-IR technology. X-ray diffraction patterns of the samples were done by an X' Pert Pro (PerkinElmer, Netherland) diffractometer, with Cu Kα radiation (λ =1.54060 Å), Generator settings = 40 kV, 40 mA and the 2θ range from 10 to 80 °C. The average dimension (D) of particles was calculated based on the diffraction of peak broadening using the Debye–Scherrer's Eq. (2) [37]:

$$D = \frac{k\lambda}{\beta cos\theta} \quad (2)$$

Where λ is the X-ray wavelength of the Cu Kα radiation (nm), β is the peak width of the diffraction peak profile at half the maximum height resulting from the small crystallite size (radians), and K is a coefficient relating to the crystalline shape and is normally equal to 0.9.

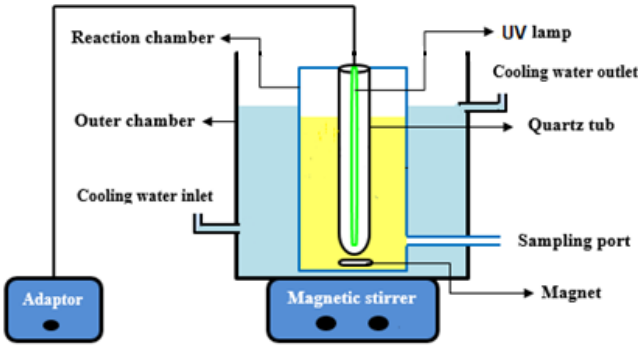

Fig. 1. The schematic diagram of the experimental reactor used for photocatalysis.

The morphological features and surface characteristics of TiO_2 were investigated using a FESEM unit (MIRA3, TE-SCAN, Czechoslovakia). FT-IR, is another characterization technique that was obtained using Spectrum Tow PerkinElmer, USA. Statistical analysis also was carried out using the software R.

2.3. Experimental design with RSM

RSM is an efficient statistical tool used in the data analysis, statistical design of the experiments, and optimizing the operating conditions in independent variables [38]. In RSM, two designs are used, they are Box Behnken Design (BBD) and Central Composite Design (CCD). In this survey, for predicting and modeling the complicated relations between input-independent factors (pH(X_1), the initial dye concentration (X_2), reaction time (X_3), TiO2 dose (X_4), and temperature (X_5)) and determining the dye removal efficiency(Y) under the optimum operational conditions several of experiments were accomplished according to a CCD [39]. The actual values of the independent variables applied to the experimental design are shown in Table 1.

The Independent variables were different over three levels as -1, 0, and 1, respectively at the specified ranges based on a set of preliminary experiments.

Table 1. Coded values of independent variables used for experimental design.

Variable		Coded level		
		-1	0	1
		values		
pH	x_1	2	6.5	11
TiO_2 (g L^{-1})	x_2	0.2	50.7	1.2
Time (min)	x_3	15	67.5	120
Temp (°C)	x_4	20	40	60
Conc. DB71 (mg L^{-1})	x_5	10	55	100

The experimental design was done using R software for Windows (version 3.0.3:6 March 2014). The total number of experiments according to *Eq.* (3) were done for the five factors.

No. of experiments = $2^k + 2k + 20$ **(3)**

Totally, 62 runs were considered using a 32 full factorial design (the base design), 10 axial points and 20 replicates in the center point [40].

A quadratic model as *Eq. (4)* was applied to express the interaction between (*Y*) and (X_1, X_2, X_3, X_4 and X_5):

$$\gamma = B_0 + \sum_{i=1}^{k} B_i X_I + \sum_{I=1}^{K} B_{ii} X_i^2 + \sum_{i=1}^{k-1} \sum_{j=1}^{k} B_{IJ} X_I X_J + C \quad \textbf{(4)}$$

Where B_0 is the intercept value, B_i, B_{ii}, and B_{ij} refer to the regression coefficient for linear, second order, and interactive effects respectively, X_i and X_j are the independent variables, and C denotes the error of prediction [41,42].

3. Results and Discussion

3.1. Characterization of the TiO_2 nanoparticles

To survey the structure, nature and size of TiO_2 crystalline phases, XRD analysis was performed (Fig. 2). The XRD analysis demonstrates the diffraction pattern and the mineralogical composition of the TiO_2 nanoparticles. According to the Eq. (2), the average crystallite size based on the half width of the most intense peak (101) was estimated to be 30 nm, suggesting achievement to nanoscale crystals. As shown in Fig. 2, several Titania crystalline peaks for samples can be seen at 2θ including 25.4(101), 37.9(004), 48.0(200), 54.5(211), 62.6(204), 69.5(116) and 75.2(118) [JCPDS No. 71-1167 were a = 3.786 Å and c = 9.507Å] which shows the existence of the anatase phase [43].

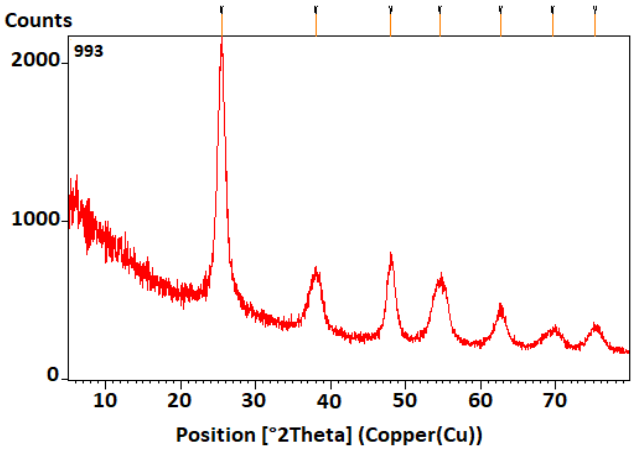

Fig. 2. XDR pattern of TiO_2 nanoparticles.

The FESEM provides topographical and elemental information with the virtually unlimited depth of fields. The FESEM images of the TiO_2 nanoparticles before (A) and after (C) degradation process are shown in Fig. 3. As shown in Fig. 3A, nanoparticles are spherical and dispersed in different sizes (20–60 nm). TiO_2 nanoparticles are very fine and have an irregular texture. Further, there are holes between the porous structure of this material. In some places the nanoparticles are well-set in mass, but in general, optimum scattering of particles is observed in the surface. After of the degradation process no noticeable changes were identified in the surface morphology of the TiO_2 nanoparticles (Fig. 3C). Energy-dispersive X-ray spectroscopy (EDS) is an analytical technique applied to the elemental analysis of a sample. The EDS spectra of the TiO_2 nanoparticles, before (B) and after (D) of dye removal in order to study their localized elemental information are presented in Fig. 3. Oxygen and Titania are the elements throughout the surface of the TiO_2 nanoparticles before removing the dye with weight percentages of 43.1 and 56.9 respectively (Fig. 3B).

Therefore, the presence of TiO_2 was confirmed. After removing the dye, O, Ti, C, Na, S and N are the elements throughout the surface of the TiO_2 nanoparticles with weight percentages of 35.3, 52.1, 12.5, 0.1, 0.1 and 0.0%, respectively. So, after removing the dye with TiO_2 nanoparticles, these elements are added as observed in Fig. 3D [44,45].

To inspect frequency changes in the functional group of the photocatalyst, the surface characteristics of the TiO_2 nanoparticles before and after degradation of direct blue 71 dyes, were investigated by using the Fourier transform infrared spectroscopy (FT-IR) spectra in the range of 400-4000 cm^{-1} (Fig. 4A and 4B).

The FT-IR spectrum of TiO_2 nanoparticles before the degradation of dye shows that the peak situations are at 3390, 1631, 792 cm^{-1}. The decomposition band at ~3390 cm^{-1} was the characteristic peak of alcohol and phenol groups due to the symmetric stretching vibration of OH. The intense broad peak at ~1631cm^{-1} is allocated in the bending vibration of the C=O bond. Furthermore, the small peak at ~792 cm^{-1} might be appropriate to the bending vibration of the N–H bond.

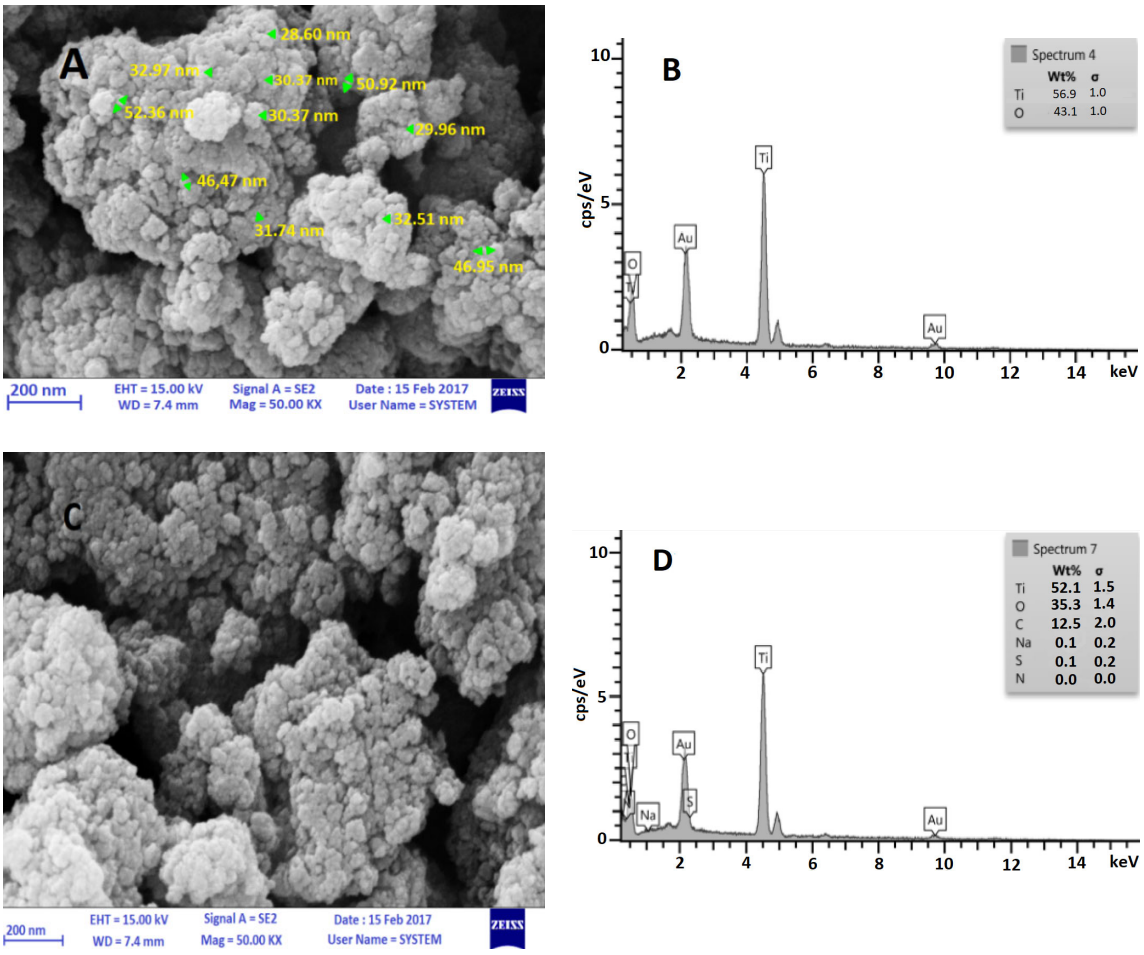

Fig. 3. FESEM image and EDS spectrum of TiO_2 nanoparticles before (A, B), and after (C, D) of dye removal.

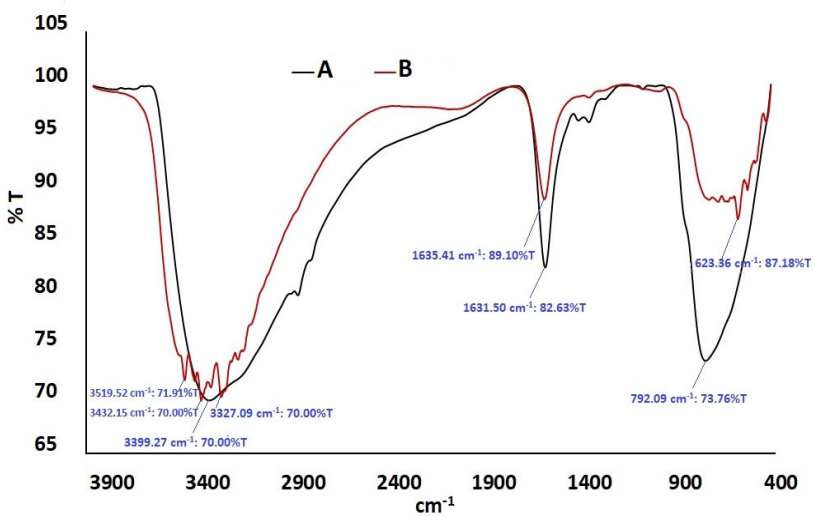

Fig. 4. FT-IR spectra of TiO_2 nanoparticles before (A), and after (B) degradation of dye.

The FT-IR spectrum of TiO_2 nanoparticles after removal of dye indicates the peak at 3519, 3492, 3327, 1635 and 623 cm^{-1}. The bonds at 3519, 3492 and 3327 specify the tensile frequencies OH from alcohol and phenol groups, 1628 presents the tensile frequency C–H from the amide group and 783 shows the bend frequency N–H from the amine group [46-48].

3.2. Quadratic models for photocatalytic degradation of dye via the TiO_2 nanoparticles

To study the individual and combined effects of variables on dye removal efficiency, degradation experiments were accomplished at the specified combinations of the physical parameters. The CCD design matrix was performed to appraise the contribution of five influential factors including pH, TiO_2 dosage, time, temperature and dye concentration. The experimental design of 62 runs along with the experimental and the predicted data for the removal of dye by TiO_2 nanoparticles in the CCD experimental design are presented in Table 2. To determine the optimum conditions, the RSM results need to be surveyed through the optimization process [49].

From Table 2, it can be observed that the dye removal values are between 17.0% (Run 38) and 90.2% (Run 48). Moreover, the lowest dye removal efficiency has been in run 38, and the main reasons for decreasing removal can be the lower pH level and/or lower TiO_2 dosage. When the TiO_2 dose and pH level are low, e.g. run 38, the synergistic efficacy was very significant and the dye removal efficiency reduced intensively. Referring to Table 2, the time and temperature have low significant effects on dye removal with TiO_2 nanoparticles. Run 48 was clear at optimum conditions, because it indicated the highest removal efficiency, and also the pH is a very essential parameter in water treatment plants. The pH, TiO_2 dosage and dye concentration were considered as optimum conditions. The pH in an acidic range may induce serious operational difficulties in water treatment processes. So, economically the conditions for run 48 with the pH 6.5, initial dye concentration of 55 mg L^{-1}, time of 67.5 min, temperature of 40 ℃ and TiO_2 dosage of 1.2 g L^{-1} are better than other runs.

3.3. Development of regression model equation and model analysis

The reduced quadratic model was produced by the multiple regression analysis of the experimental data, and are presented in Table 3. According to the Table 3, it is observable that the pH (X_1), TiO_2 dosage (X_2), time (X_3), temperature (X_4) and initial dye concentration (X_5) are significant (p-values < 0.05), so five terms available in Table 3 could affect the model formulation. In this table, it can be seen that the pH (X_1), TiO_2 dosage (X_2), time (X_3), temperature (X_4), X_1:X_2, X_1:X_5, X_2:X_3, X_2:X_4, X_3^2 and X_5^2 have synergistic effects on the response prediction by the model, while the initial dye concentration (X_5), X_1:X_3, X_2:X_5, X_3:X_5, X_1^2 and X_2^2 have antagonistic effects.

Dye removal efficiency predicted by the model is presented in the Table 2. When the response predicted by the model and experimental data obtained in the laboratory have a leaner correlation, the model is reliable [50].

The equations of quadratic model, for both coded and uncoded values of the parameters, are indicated at Eqs. (5) and (6), respectively. Therefore, these models can be applied for the purposes of prediction and optimization [51-53].

$$\gamma_{Dye}=-20.948+20.371X_1+40.173X_2-0.1251X_5+0.4916X_1X_2-0.001669X_1X_3+0.006114X_1X_5 +0.03644X_2X_3+0.06061X_2X_4-0.06001X_2X_5-0.0001748X_3X_5-1.679X_1^2-10.304X_2^2 +0.0003998X_3^2+0.0009392X_5^2 \quad (5)$$

$$\gamma_{Dye}=77.4576+11.2994X_1+14.1266X_2+2.0711X_3+0.8171X_4-1.6123X_5+1.1060X_1X_2-0.3943X_1X_3 +1.2380X_1X_5+0.9564X_2X_3+0.60608X_2X_4-1.35017X_2X_5-0.41308X_3X_5-33.9980X_1^2-3.26022X_2^2 +1.10191X_3^2+1.90191X_5^2 \quad (6)$$

Table 2. CCD experimental design for RB5 removal by TiO_2 nanoparticles.

Run	Independent factors					Removal (%)		Run	Independent factors					Removal (%)	
	X_1	X_2	X_3	X_4	X_5	Expt.	Expt.		X_1	X_2	X_3	X_4	X_5	Expt.	Pred.
1	2	1.2	120	60	100	45.3	47.59	32	2	1.2	120	20	100	42.9	44.68
2	11	1.2	120	20	10	72.4	75.46	33	11	0.2	120	60	100	41.6	43.20
3	6.5	0.7	67.5	40	55	75.7	78.84	34	6.5	0.7	67.5	40	55	77.8	78.84
4	2	1.2	15	20	100	34.6	36.61	35	11	0.2	15	60	100	39.9	40.53
5	6.5	0.7	67.5	40	55	79.6	78.84	36	2	1.2	15	60	100	38.8	39.52
6	11	1.2	120	20	100	68.8	71.18	37	11	0.2	120	20	100	39.5	40.53
7	6.5	0.7	67.5	40	55	78.4	78.84	38	2	0.2	15	60	100	17.0	16.88
8	6.5	0.7	67.5	40	55	77.9	78.84	39	2	0.2	15	20	10	18.6	18.57
9	11	0.2	15	20	100	39.7	40.04	40	11	0.2	120	60	10	41.3	42.07
10	11	1.2	15	20	10	67.3	67.31	41	6.5	0.7	67.5	40	55	78.8	78.84
11	6.5	0.7	67.5	40	55	78.2	78.84	42	2	1.2	15	60	10	47.7	47.10
12	2	0.2	120	60	100	18.9	21.13	43	6.5	0.7	67.5	40	55	77.6	78.84
13	11	1.2	120	60	10	75.9	78.36	44	6.5	0.7	67.5	40	55	76.9	78.84
14	11	0.2	15	60	10	36.8	37.75	45	6.5	0.7	67.5	40	55	76.7	78.84
15	2	0.2	15	60	10	18.2	19.06	46	2	0.7	67.5	40	55	32.5	33.54
16	6.5	0.7	67.5	40	55	77.1	78.84	47	6.5	0.7	67.5	40	55	77.3	78.84
17	2	1.2	120	20	10	50.6	53.91	48	6.5	1.2	67.5	40	55	90.2	89.70
18	11	1.2	15	60	10	69.2	70.22	49	6.5	0.7	67.5	40	55	76.8	78.84
19	6.5	0.7	67.5	40	55	77.1	78.84	50	6.5	0.7	67.5	40	55	77.9	78.84
20	2	1.2	120	60	10	54.4	56.82	51	6.5	0.7	15	40	55	75.3	76.84
21	11	1.2	120	60	100	70.9	74.09	52	6.5	0.7	67.5	40	10	80.8	82.35
22	11	1.2	15	60	100	67.5	67.59	53	6.5	0.7	67.5	20	55	77.5	77.99
23	11	0.2	120	20	10	38.7	41.59	54	11	0.7	67.5	40	55	54.3	56.13
24	11	1.2	15	20	100	65.3	64.68	55	6.5	0.7	67.5	40	55	75.7	78.84
25	2	0.7	120	20	10	40.7	42.45	56	6.5	0.7	67.5	40	55	77.1	78.84
26	6.5	0.2	67.5	40	55	58.7	61.45	57	6.5	0.7	67.5	40	55	76.7	78.84
27	2	1.2	15	20	10	43.8	44.19	58	6.5	0.7	67.5	60	55	77.3	79.68
28	2	0.2	120	20	100	17.5	20.64	59	6.5	0.7	67.5	40	100	77.8	79.12
29	11	0.2	15	20	10	37.7	37.27	60	6.5	0.7	67.5	40	55	78.3	78.84
30	2	0.2	120	60	10	21.9	24.95	61	6.5	0.7	120	40	55	81.7	83.04
31	2	0.2	15	20	100	17.2	16.30	62	6.5	0.7	67.5	40	55	77.4	78.84

X_1: pH, X_2: TiO_2 (g L^{-1}), X_3: Time (min), X_4: Temperature (°C), X_5: dye concentration (mg L^{-1}).

Table 3. Regression analysis for the reduced quadratic model.

Model term	Coefficient estimate	Std. error	t-Value	p-Value
Intercept	77.45760	0.19204	403.3432	2.2×10^{-16}
X_1	11.29945	0.17068	66.2043	2.2×10^{-16}
X_2	14.12663	0.17324	81.5417	2.2×10^{-16}
X_3	2.07114	0.17068	12.1349	8.669×10^{-16}
X_4	0.81710	0.17068	4.7874	1.860×10^{-05}
X_5	-1.61231	0.17068	-9.4467	2.999×10^{-12}
$X_1:X_2$	1.10608	0.17882	6.1853	1.656×10^{-07}
$X_1:X_3$	-0.39433	017601	-2.2404	0.030048
$X_1:X_5$	1.23808	0.17601	7.0341	9.070×10^{-09}
$X_2:X_3$	0.95642	0.17882	5.3485	2.860×10^{-06}
$X_2:X_4$	0.60608	0.17882	3.3893	0.001467
$X_2:X_5$	-1.35017	0.17882	-7.5504	1.568×10^{-09}
$X_3:X_5$	-0.41308	0.17601	-2.3469	0.023390
X_1^2	-33.99809	0.60026	-56.6387	2.2×10^{-16}
X_2^2	-3.26022	0.54069	-6.0298	2.82×10-07
X_3^2	1.10191	0.60026	1.8357	0.073013
X_5^2	1.90191	0.60026	3.1685	0.002754

The model adequacy can be described by ANOVA analysis, R^2 and R^2adj that are shown in Table 4. In the ANOVA analysis via high F, the low p-value, correlation coefficient (R), and the results of lack of a fit test can be predicted by statistical significance and accuracy of the models [54]. Also the p-value less than 0.05 indicates the model terms are significant and the values greater than 0.10 shows they are not significant. The lack of fit value parameters indicates the variation of response around the fitted model; if the model fits data well this parameter should be insignificant [55]. According to the ANOVA analysis, the higher *F*-value of 1832 with a *p*-value lower than 0.0001 indicates that the second-order polynomial model is statistically significant as shown in Table 4, thus the model fitted the experimental results well.

Table 4. Analysis of variance (ANOVA) for the reduced quadratic model.

Model formula in RSM X_1, X_2, X_3, X_4, X_5	DF	Sum of squares	Mean square	F-value	$F_{critical}$	Probability (P)
First-order response	5	10487.4	2097.5	2150.244	4.45	2.2×10^{-16}
TWI(x1, x2)	1	82.5	82.5	84.575		6.704×10^{-12}
TWI(x1, x3)	1	10.8	10.8	11.115		0.0017207
TWI(x1, x5)	1	65.2	65.2	66.885		1.899×10^{-10}
TWI(x2, x3)	1	4.3	4.3	4.405		0.0414764
TWI(x2, x4)	1	47.2	47.2	48.365		1.190×10^{-08}
TWI(x2, x5)	1	17.1	17.1	17.574		0.0001276
TWI(x3, x5)	1	11.9	11.9	12.194		0.0010869
Pure quadratic response	4	17870.1	4467.5	4579.927		2.2×10^{-16}
Residuals	45	43.9	1.0			
Lack of fit	26	26.3	1.0	1.097	2.1	0.423997
Pure error	19	17.5	0.9			

Notes: Multiple R-squared: 0.9985, Adjusted R-squared: 0.9972, F-statistic: 1832 on 16 and 45 DF, p-value: $< 2.2\times10^{-16}$.

The F-values of linear and quadratic terms of the model are 2150.24 and 4579.92 respectively, this shows the model and the individual coefficients of the model are more significant. F-value of model is significant (F_{cal} = 2150.24 > $F_{0.05, 5, 45}$ = 4.45) and the lack of the fit value of the model available in Table 4, is not significant relative to the pure error (F_{cal} = 1.09 < $F_{0.05, 26, 19}$ = 2.1), they indicated the correlation between factors and dye removal as a response [56,57].

In general, the efficiency of the model is illustrated by the R^2 value of 0.9972. On the other hand, R^2 values (R^2 = 0.9985, adjusted R^2 = 0.9972, predicted R^2 = 0.9974) are close to one and indicated that about 99% of the variations presented in the results can be described by the independent variables and their interaction effects. Also R^2 values showed a satisfactory adjustment between quadratic model and experimental data [58,59]. Pareto analysis using the Eq. (7) was employed to assess the importance of the role (P_i) of the selected factors (factor i) of the created response.

$$P_i = \left(\frac{\beta_i^2}{\sum \beta_i^2}\right) \quad (7)$$

As indicated in Fig. 5, the following sequence was gained for the terms containing singular factors X_2 (TiO_2; 13.2%) > X_1 (pH, 8.4%) > X_3 (Time; 0.3%) > X_5 (Temp; 0.17%) > X_4 (Conc.DB71; 0.044%), which proves that TiO_2 and pH play the most important role among these terms. The quadratic terms have the sequence of X_1^2 (74.4%) > X_2^2 (10.6%) > X_5^2 (0.23%) > X_3^2 (0.08%), while the interaction terms have the sequence of X_2X_5 (0.12%) > X_1X_5 (0.1%) > X_1X_2 (0.08%) > X_2X_3 (0.06%) > X_2X_2 (0.02%) > X_3X_5 (0.01%) > X_1X_3 (0.01). So the quadratic pH and the TiO_2-Conc. DB71 interaction play the most important role in the created response. The results obtained from the Pareto method can be well confirmed by the F-values [60,61].

3.4. Response surface methodology and contour plotting

To study the effects of various parameters and their interactions on the efficiency of the dye decomposition via TiO_2 nanoparticles, the contour plots which is specified based on the model coefficients is shown in Fig. 5 (A-F). In these plots, the effect of two variables is studied while the other parameters are stabilized [62]. The effect of TiO_2 dosage and pH solution on the removal efficiency at the initial time of 67.5 min, temperature of 40 °C and dye concentration of 55 mg L^{-1} is presented in Fig 6A. The percentage of dye removal was changed by varying the TiO_2 dosage and pH. As can be understood from the figure, in the neutral pH, the increase of the TiO_2 dosage, led to the increase of removal efficiency from 60 to 80%. This reveals that the pH and TiO_2 dosage play an important role in the decomposition process [63]. Fig. 6B indicates the effects of the pH and contact time in the removal efficiency of photocatalyst process. Based on this image in the pH range of 7, dye degradation was increased by the time increase. The interaction effects of pH (X_1) and dye concentration (X_5) in Fig. 6C shows that the percentage of dye removal was decreased with increasing dye concentration. Fig. 6D presents that dose of the catalyst and the contact time have synergistic effects, so that the increase of the TiO_2 dosage and contact time can enhance removal efficiency up to 90%. The interaction effects of the TiO_2 dosage (X_2) and dye concentration (X_5) are presented in Fig. 6E. This figure shows that the interaction X_2X_5 had antagonistic effects. Fig. 6F also indicates the combined effects of the contact time and dye concentration. As shown, dye photodegradation was increased with the increase of the contact time. Based on the results, it is clear that the TiO_2 dosage, pH and dye concentration are the most effective variables in the dye removal efficiency [64, 65].

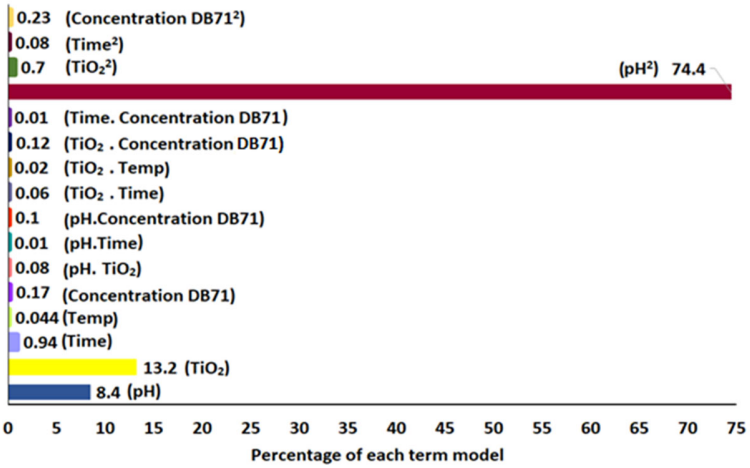

Fig. 5. Pareto plot for studying the importance of each variable to the TiO_2 response in the removal of dye.

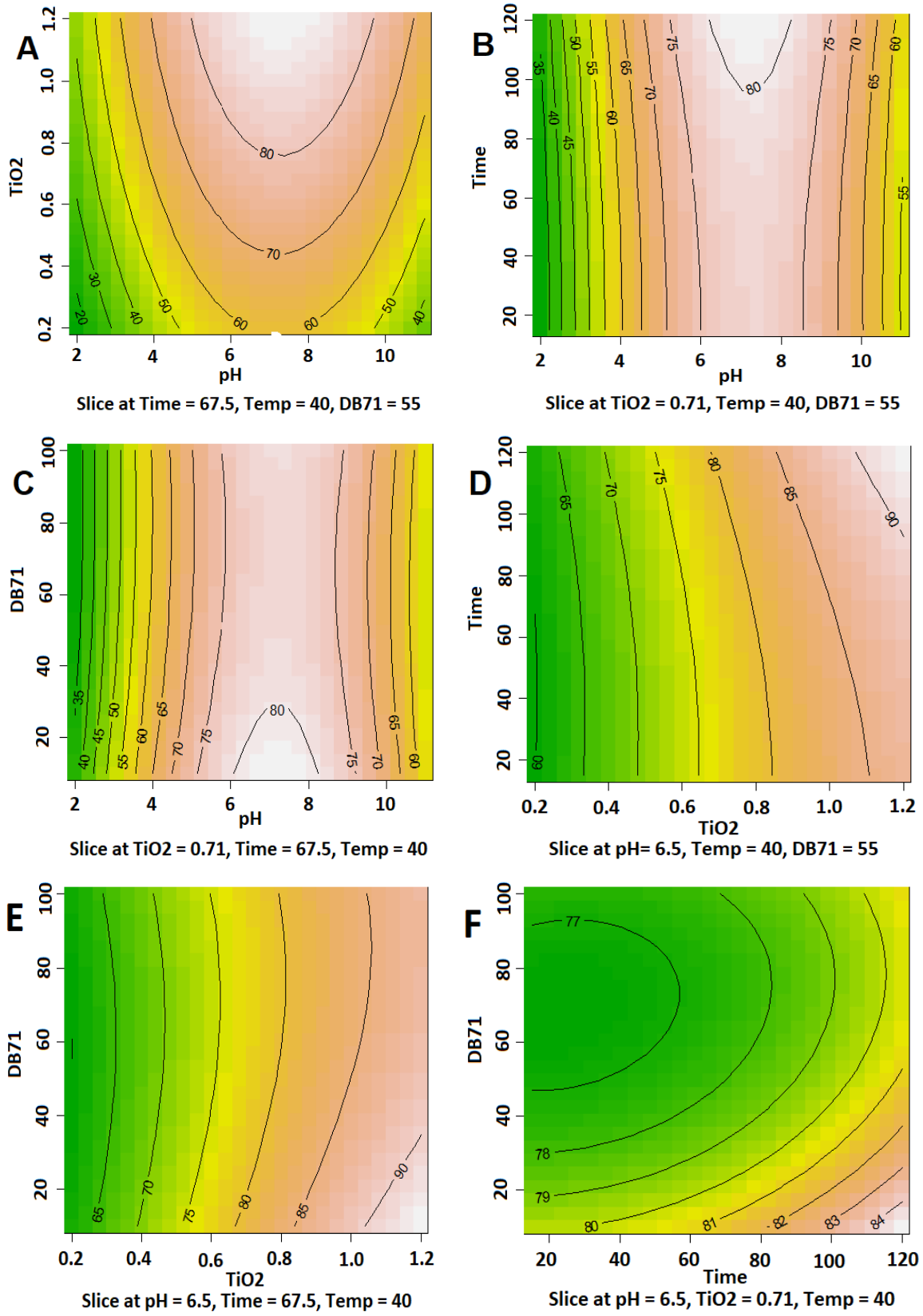

Fig. 6. Contour plot for the effect of TiO_2 dosage and pH (A), pH and Time (B), pH and Dye concentration (C), TiO_2 dosage and Time (D), TiO_2 dosage and Dye concentration (E), Time and Dye concentration (F).

3.5. Process optimization and confirmation

The Solver "Add-ins" was applied by effective parameters to achieve the optimum decomposition conditions through the model equation predicted by RSM. These parameters included pH (2-11), TiO_2 dosage (0.2-1.2 g L^{-1}), contact time (15-120 min), temperature (20-60 ℃) and the initial dye concentration (10-100 mg L^{-1}). In the optimum conditions, all parameters simultaneously are favorable criteria, and in the predicted optimal conditions, the maximum removal efficiency was calculated to be 100 %. The predicted optimal conditions by the Solver "Add-ins" were the pH of 7.43, TiO_2 dosage of 1.17 g L^{-1}, contact time of 120 min, temperature 49.63℃ and initial dye concentration of 17.73 mg L^{-1}.

To confirm the validity of the predicted optimum conditions, laboratory experiments were performed and the findings showed that the experimental data were in good agreement with the above-mentioned optimal conditions [66-68]. To confirm the validity of the results predicted by the model, additional laboratory experiments were done in four replicates. As it can be seen in Table 5, experimental data were in consistent with those predicted through the regression model. Additionally, there is another set of experiments shown in Table 5, they have same optimal conditions except for initial pH.

The result shows that the R-squared value of the model is very close to the adjusted R-squared value. The presence of significant terms in the model was certified by the good agreement between R^2 adj. (0.99) and R^2 pred. (0.99) indicated in Fig. 7 [69].

4. Conclusions

In this study, the decomposition of dye via TiO_2 nanoparticle at the solid/aqueous interface was investigated. The CCD design matrix was done to study the relationship between input-independent factors (pH, TiO_2 dose (g L^{-1}), contact time (min), temperature (℃), and dye concentrations (mg L^{-1})) and one dependent output response (removal efficiency) on dye decomposition with TiO_2 photocatalyst. The quadratic equations developed for this survey show a good correlation between actual and model predicted values of response. The results such as p-value (2.2×10^{-16}), higher F-value (1832), R^2 (multiple R-squared: 0.9985, adjusted R-squared: 0.9972), insignificant lack of fit (0.423) indicate that the reduced full second order model is highly significant for dye removal by TiO_2 nanoparticles. The closeness of the R-squared value of the model to the adjusted R-squared value shows that the quadratic regression related to the reduced full second order model can be used for prediction and optimization.

Table 5. Experimental and predicted values of the responses at the optimal levels predicted by RSM.

pH	TiO_2 (g L^{-1})	Time (min)	Temp (℃)	Dye concentration (mg L^{-1})	Phosphate removal (%)	
					Predicted	Experimental
6.5	1.2	67.5	40	55	89.7	90.2
9	1.2	67.5	40	55	86.1	84.7

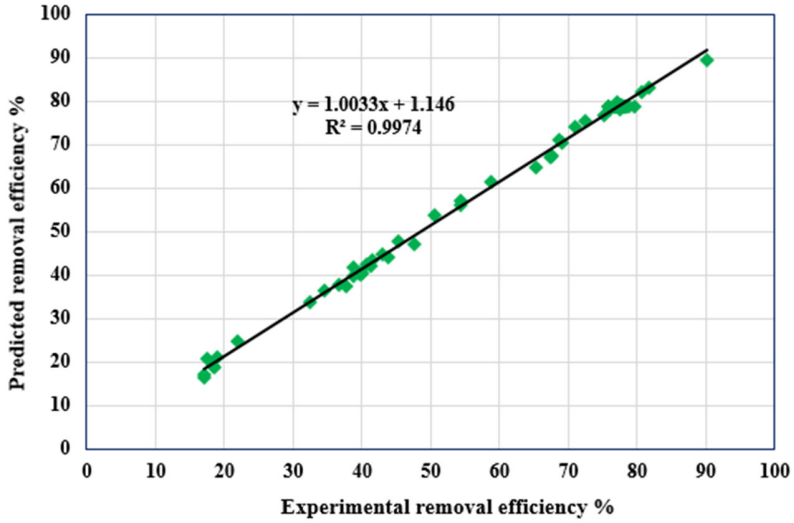

Fig. 7. Correlation of actual and predicted removal efficiency for dye direct blue 71.

The maximum percentage of removal of dye, 90.2%, was gained at optimum operating conditions including pH=6.5, TiO_2 dose (1.2 g L^{-1}), contact time (67.5 min), temperature (40 °C), and dye concentrations (55 mg L^{-1}). The maximum removal efficiency was anticipated to be 100%, using regression coefficients achieved by the model and Solver "Add-ins". Therefore, the results show that the photocatalytic process is very effective in removing dye from contaminated water, and it has good efficiency in eliminating textile dyes. Hence we suggest that this catalyst will be used in treatment of different dye pollutants.

Acknowledgements

This study is related to the project NO 904003/81 from the Student Research Committee, Ilam University of Medical Sciences, Ilam, Iran. We also appreciate the "Student Research Committee" and "Research & Technology Chancellor" in Ilam University of Medical Sciences for their financial support of this study.

References

[1] G. Manikandan, P.S. Kumar, A. Saravanan, J. Ind. Eng. Chem. 62 (2018) 446-461.
[2] P. Sharma, H. Kaur, M. Sharma, V. Sahore, Environ. Monit. Assess. 183 (2011) 151-195.
[3] I. Guerrero-Coronilla, L. Morales-Barrera, T.L. Villegas-Garrido, E. Cristiani-Urbina, Environ. Eng. Manag. J. 13 (2014) 1917-1926.
[4] I. Guerrero-Coronilla, L. Morales-Barrera, E. Cristiani-Urbina, J. Environ. Manage. 152 (2015) 99-108.
[5] M.A. Hassaan, A. El Nemr, F.F. Madkour, Egypt. J. Aquat. Rese. 43 (2017) 11-19.
[6] Y. Du, M. Pei, Y. He, F. Yu, W. Guo, L. Wang, PloS One. 9 (2014) 1160-1173.
[7] S. Arivoli, M. Thenkuzhali, P. Martin Deva Prasath, Orbital: Electron. J. Chem. 1 (2009) 138-155.
[8] W. Li, D. Li, Z. Chen, H. Huang, M. Sun, Y. He, X. Fu, J. Phys. Chem.C 112 (2008) 14943-14947.
[9] V. Belessi, G. Romanos, N. Boukos, D. Lambropoulou, C. Trapalis, J. Hazard. Mater. 170 (2009) 836-844.
[10] P.V. Nidheesh, M. Zhou, M.A. Oturan, Chemosphere 197 (2018) 210-227.
[11] A. Srinivasan, T. Viraraghavan, J. Environ. Manage. 91 (2010) 1915-1929.
[12] A. Bhatnagar, A.K. Minocha, Environ. Technol. 31 (2010) 97-105.
[13] L. Shabani, H. Aliyan, Iran. J. Catal. 6 (2016) 221-228.
[14] S. Liu, C. Ni, H. Su, H. Liu, R. Chen, P. Li, Y. Wei, RSC Adv. 6 (2016) 30840-30845.
[15] Y. Jiang, Y. Luo, F. Zhang, L. Guo, L. Ni, Appl. Surf. Sci. 273 (2013) 448-456.
[16] M. Bayat, V. Javanbakht, J. Esmaili, Int. J. Biol. Macromol. 116 (2018) 607-619.
[17] C-H. Liang, F-B. Li, C-S. Liu, J-L. Lü, X-G. Wang, Dyes Pigm. 76 (2008) 477-484.
[18] P. Muthirulan, C. Nirmala Devi, M. Meenakshi Sundaram, Arab. J. Chem. 10 (2017) 1477-1483.
[19] J. Marugán, M-J. López-Muñoz, R. van Grieken, J. Aguado, Ind. Eng. Chem. Res. 46 (2007) 7605-7610.
[20] N. Ajoudanian, A. Nezamzadeh-Ejhieh, Mater. Sci. Semicond. Process. 36 (2015) 162-169.
[21] M. Babaahamdi-Milani, A. Nezamzadeh-Ejhieh, J. Hazard. Mater. 318 (2016) 291-301.
[22] H, Derikvandi, A. Nezamzadeh-Ejhieh, J. Hazard. Mater. 321 (2017) 629-638.
[23] E. Kordouli, K. Bourikas, A. Lycourghiotis, C. Kordulis, Catal. Today 252 (2015) 128-135.
[24] M.M. Amin, F. Teimouri, M. Sadani, M.A. Karami, Desalin. Water Treat. 57 (2016) 9455-9464.
[25] M.M. Amin, B. Jaberian, B. Bina, M. Sadani, R. Hadian, G. Bonyadinejad, M.M. Ahmad Moazzam, EnvironmentAsia 7 (2014) 57-64.
[26] N. Hidayati Othman, N. Hashimah Alias, M. Zaman Shahruddin, N. Fitrah Abu Bakar, N. Raikhan Nik Him, W.J. Lau, J. Environ. Chem. Eng. 6 (2018) 2803-2811.
[27] J. Esmaili-Hafshejani, A. Nezamzadeh-Ejhieh, J. Hazard. Mater. 316 (2016) 194-203.
[28] H. Zangeneh, A.A.L. Zinatizadeh, M. Habibi, M. Akia, M. Hasanain Isa, J. Ind. Eng. Chem. 26 (2015) 1-36.
[29] A. Pirkarami, M.E. Olya, S. Raeis Farshid, Water Resour. Ind. 5 (2014) 9-20.
[30] M.M. Ba-Abbad, A.A.H. Kadhum, A.B. Mohamad, M.S. Takriff, K. Sopian, Int. J. Electrochem. Sci. 7 (2012) 4871-4888.
[31] A. Nezamzadeh-Ejhieh, M. Bahrami, Desalin. Water Treat. 55 (2015) 1096-1104.
[32] H. Zabihi-Mobarakeh, A. Nezamzadeh-Ejhieh, J. Ind. Eng. Chem. 26 (2015) 315-321.
[33] S.A. Hosseini, R. Saeedi, Iran. J. Catal. 7 (2017) 37-46.
[34] M. Nosuhi, A. Nezamzadeh-Ejhieh, Electrochim. Acta 223 (2017) 47-62.
[35] A.Y. Shan, T.I.M. Ghazi, S.A. Rashid, Appl. Catal. A 389 (2010) 1-8.
[36] P. Patnaik, Handbook of Environmental Analysis, 2nd ed, CRC Press, Boca Raton, 2010.
[37] S. Aghabeygi, R. Kiakojori, H. Vakiki Azad, Iran. J. Catal. 6 (2016) 275-279.
[38] K. Rajkumar, M. Muthukumar, Environ. Sci. Pollut. Res. 19 (2012) 148-160.
[39] S. Ghafoori, A. Mowla, R. Jahani, M. Mehrvar, P.K. Chan, J. Environ. Manage. 150 (2015) 128-137.
[40] A. Mohseni Bandpei, S.M. Mohseni, A. Sheikhmohammadi, M. Sardar, M. Sarkhosh, M. Almasian, M. Avazpour, Z. Mosallanejad, Z. Atafar, S. Nazari, S. Rezaei, Korean J. Chem. Eng. 34 (2017) 376-383.
[41] S. Sadri Moghaddam, M.A. Alavi Moghaddam, M. Arami, J. Hazard. Mater. 175 (2010) 651-657.
[42] A.T. Nair, A.R. Makwana, M. Mansoor Ahammed, Water Sci. Technol. 69 (2014) 464-478.
[43] Z.M. Abou-Gamra, M.A. Ahmed, Adv. Chem. Eng. Sci. 5 (2015) 373-388.
[44] Y. Park, Z. Sun, G.A. Ayoko, R.L. Frost, Chemosphere 107 (2014) 249-256.

[45] H. Godini, F. Hashemi, L. Mansuri, M. Sardar, G. Hassani, S. Mohseni, A.A. Alinejad, S. Golmohammadi, A. Sheikh Mohammadi, J. Water Reuse Desalin. 6 (2016) 544-552.
[46] J. Petroski, M.A. El-Sayed, J. Phys. Chem. A 107 (2003) 8371-8375.
[47] S. Wang, S.P. Jiang, X. Wang, Electrochim. Acta 56 (2011) 3338-3344.
[48] W. Konicki, M. Aleksandrzak, D. Moszyński, E. Mijowska, J. Colloid Interface Sci. 496 (2017) 188-200.
[49] H. Aslani, R. Nabizadeh, S. Nasseri, A. Mesdaghinia, M. Alimohammadi, A.H. Mahvi, N. Rastkari, S. Nazmara, Desalin. Water Treat. 57 (2016) 25317-25328.
[50] S. Ghafari, A.A Hamidi, M. Hasanian Isa, A.A. Zinatizadeh, J. Hazard. Mater. 163 (2009) 650-656.
[51] K.K. Garg, B. Prasad, J. Taiwan Inst. Chem. Eng. 60 (2016) 383-393.
[52] M. Umar, A.A Hamidi, M.S. Yusoff, Desalination 274 (2011) 278-283.
[53] M. Mansoor Ahammed, S. Dave, A.T. Nair, Desalin. Water Treat. 56 (2015) 315-326.
[54] T.V. Thuan, B.T. Phuong Quynh, T.D. Nguyen, V.T. Thanh Ho, L.G. Bach, Surf. Interface 6 (2017) 209-217.
[55] G. Hassani, A. Takdastan, M. Ghaedi, G. Goudarzi, A. Neisi, A.A. Babaei, Int. J. Electrochem. Sci. 11 (2016) 8471-8485.
[56] S. Senobari, A. Nezamzadeh-Ejhieh, J. Mol. Liq. 261 (2018) 208-217.
[57] M. Nosuhi, A. Nezamzadeh-Ejhieh, J. Electroanal. Chem. 810 (2018) 119-128.
[58] S. Senobari, A. Nezamzadeh-Ejhieh, J. Mol. Liq. 257 (2018) 173-183.
[59] M. Nosuhi, A. Nezamzadeh-Ejhieh, New J. Chem. 41 (2017) 15508-15516.
[60] Z. Amani-Beni, A. Nezamzadeh-Ejhieh, New J. Chem. 42 (2018) 1021-1030.
[61] H. Derikvandi, A. Nezamzadeh-Ejhieh, J. Colloid Interface Sci. 490 (2017) 628-641.
[62] S.S. Chong, A.R. Abdul Aziz, S.W. Harun, H. Arof, S. Shamshirband, Measurement 74 (2015) 78-86.
[63] F. Nasiri Azad, M. Ghaedi, K. Dashtian, A. Jamshidi, G. Hassani, M. Montazerozohori, S. Hajati, M. Rajabi, A.A. Bazrafshan, RSC Adv. 6 (2016) 19780-19791.
[64] H. Derikvandi, A. Nezamzadeh-Ejhieh, J. Colloid Interface Sci. 490 (2017) 652-664.
[65] H. Derikvandi, A. Nezamzadeh-Ejhieh, J. Photochem. Photobiol. A: Chem. 348 (2017) 68-78.
[66] J. Wu, D. Yu, H. Sun, Y. Zhang, W. Zhang, F. Meng, X. Du, Ind. Crops Prod. 69 (2015) 68-75.
[67] M. Naserifar, S.M. Msoudpanah, S. Alamolhoda, J. Ultrafine Grained Nanostruct. Mater. 51 (2018) 26-31.
[68] T-S. Chen, R-W. Tsai, Y-S. Chen, K-L. Huang, Int J Electrochem. Sci. 9 (2014) 8422-8434.
[69] D. Podstawczyk, A. Witek-Krowiak, A. Dawiec, A. Bhatnagar, Ecol. Eng. 83 (2015) 364-379.